

Using the T-Matrix Method for Light Scattering Computations by Non-axisymmetric Particles: Superellipsoids and Realistically Shaped Particles

Thomas Wriedt*

(Received: 29 January 2002; accepted: 10 May 2002)

Abstract

Light scattering by non-axisymmetric particles is commonly needed in particle characterization and other fields. After much work devoted to volume discretization methods to compute scattering by such particles, there is renewed interest in the T-matrix method. We extended the *null-field method with discrete sources* for

T-matrix computation and implemented the superellipsoid shape using an implicit equation. Additionally, a triangular surface patch model of a realistically shaped particle can be used for scattering computations. In this paper some exemplary results of scattering by non-axisymmetric particles are presented.

Keywords: discrete sources, light scattering, superellipsoid, T-matrix method

1 Introduction

In optical particle characterization, light scattering computations are commonly needed. They help in the design of new instruments or in the investigation of the influence of various particle characteristics, such as shape, refractive index, composition or surface roughness, on a specific optical particle sizing instrument. Various other parameters of the instrument can also be easily investigated using light scattering simulations. For instance, the effect of the wavelength of the incident laser beam, the effect of particle trajectory through a measurement volume or the influence of the Gaussian intensity distribution of a laser beam can be computed. There is continuous interest in particle shape characterization. This would help to tell apart, e.g., non-spherical particles from spherical particles or fibrous particles from other particles. To develop new instruments for particle shape recognition, of course light scattering theories and corresponding computer programs for non-spherical particles are needed. The different methods available in this field have recently been reviewed by *Wriedt* [1] and *Jones* [2]. For this introduction, the various theories can be divided into volume-based and surface-based

theories. Well known volume discretization methods are the various integral equation methods such as the discrete dipole approximation (DDA) [3], the volume integral equation method (VIEM) [4] and the differential equation method finite difference time domain method (FDTD)[5, 6]. Because the whole volume of a scatterer is discretized, the computer time is rather long. Nevertheless, these methods have been applied to compute scattering by non-spherical particles in optical particle sizing and in other fields. Scattering by cubic crystals has been studied using DDA [3] and scattering by ice crystals has been investigated using FDTD [5].

Since only the surface of a scattering body is discretized, the computer demand should be lower with surface-based methods, but these methods have not yet been much applied to the computation of scattering by arbitrarily shaped particles.

The T-matrix method (also called the null field method or extended boundary condition method) is the best known of these methods because fast computer codes are easily available [7, 8], but it is mainly applied to scattering by axisymmetric scatterers. The T-matrix method was originally developed by *Waterman* [9–11]. The T-matrix is based on expansion of all fields – the incident, transmitted and the scattered field – into a series of spherical vector wavefunctions.

A crucial advantage of the null-field method is that the transition matrix or the T-matrix relating the scattered

* Dr.-Ing. T. Wriedt, Institut für Werkstofftechnik, Badgasteiner Str. 3, 28359 Bremen (Germany).
E-mail: thw@iwt.uni-bremen.de

and the incident field coefficients can be computed in an easy manner. The T-matrix depends only on the incident wavelength and particle shape, its refractive index and its relation to the coordinate system. Thus, knowing a T-matrix, scattering by a rotated particle, a system of particles, a particle on a plane surface, in an incident Gaussian laser beam and orientation averaged scattering can easily be computed.

Taking into account the general properties of the T-matrix, *Mishchenko* elaborated an efficient analytical method for computing orientationally averaged light scattering characteristics for ensembles of non-spherical particles [12]. On the other hand, the T-matrix for a single scatterer can be used successfully for solving a large class of boundary-value problems in electromagnetic scattering theory. In this context, we mention the analysis of multiple scattering problems [13, 14] and the simulation of light scattering by layered or composite objects [15–17] and by particles deposited on a surface [18].

However, for particles with extreme geometries or particles with appreciable concavities, the single spherical coordinate based null-field method fails to converge. A number of modifications to the conventional null-field method have been suggested for improving the numerical stability. These techniques include formal modifications of the single spherical coordinate-based null-field method [19–21], different choices of basis functions [22, 23] and the application of the spheroidal coordinate formalism [24, 25]. One of these formal modifications is the *null-field method with discrete sources* [26–28]. Essentially, this method entails the use of a number of elementary sources for approximating the surface current densities. The discrete sources are placed on a certain support in an additional region with respect to the region where the solution is required. Unknown discrete sources amplitudes which produce the surface densities are computed by using the null-field condition of the total electric field inside the particle surface. With this method, computation of the scattering by highly elongated or flat scatterers such as fibres and plates [29] and layered particles [30] is easily possible and the standard T-matrix can also be computed [31] for post-processing such as cluster scattering or orientation averaging.

Some brief comments on the history of the T-matrix method for non-axisymmetric particles may be of interest. Early scattering computations for non-axisymmetric scatterers using the T-matrix method were done by *Barber* [32] and by *Schneider* and *Peden* [33], both presenting results for ellipsoids.

The *null field method with discrete sources* has also been extended for the computation of scattering by non-axisymmetric scatterers [34] and the method has been fully tested by comparison with other methods [35], giving results for cubes.

A 3D variant of the T-matrix method has also been developed by *Laitinen* and *Lumme* [36] and by *Kahnert* et al. [37], both presenting scattering results for rounded cubes, and another one by *Havemann* and *Baran* [38], giving results for hexagonal ice crystals.

To describe the scattering body using smooth functions, *Laitinen* and *Lumme* [36] expanded the surface of the scattering cube into a series of spherical harmonics. The problem with this method is that artificial roughness is introduced in addition to rounding of the edges of the cube. In optical particle characterization, mainly computations of scattering by some basic particle shapes have been investigated, such as spheres, spheroids, ellipsoids, cubes and finite cylinders. Because there is a lack of tools to describe particle shape, in the following the superellipsoid is proposed to generate various interesting particle shapes and it is integrated into the *null field method with discrete sources*.

The structure of the paper is arranged as follows. First the superellipsoid particle shape is described; next the *null field method with discrete sources* is briefly introduced and finally some examples of computational results are presented.

2 Superellipsoid

The superellipsoid represents a family of three-dimensional shapes as the product of two superquadratic curves [40]. This shape is well known in computer graphics and it can be used to model a wide range of shapes such as spheres, ellipsoids and cylinders and especially cubes and cylinders with rounded edges [39]. The superellipsoid is implemented in various computer programs used in computer graphics such as POV-Ray, so that a visualization of its form is easily available. The superellipsoid or superquadratic ellipsoid might be considered a generalization of the ellipsoid, and its implicit form is given by the equation

$$\left[\left(\frac{x}{a}\right)^{2/e} + \left(\frac{y}{b}\right)^{2/e}\right]^{e/n} + \left(\frac{z}{c}\right)^{2/n} - 1 = 0. \quad (1)$$

We use the same nomenclature as in POV-Ray. n is the north-south roundedness, e is the east-west roundedness and the bounds in x , y , z are given by the parameters a , b , c . The parametric form of the equation may also be useful in the construction of an object. The parametric equation of the superellipsoid is given by

$$\begin{aligned} x &= a \cos^n(\vartheta) \cos^e(\varphi) \\ y &= b \cos^n(\vartheta) \sin^e(\varphi) \\ z &= c \sin^n(\vartheta) \\ \vartheta &: [-\pi/2, \pi/2], \varphi: [-\pi, \pi]. \end{aligned} \quad (2)$$

If n and e are not equal to 1, the angles ϑ, φ of course no longer correspond to the coordinates of the spherical coordinate system. A problem would arise in the equation if $\cos(t)$ or $\sin(t)$ was negative. In this case a negative number could have a fractional exponent, which is an illegal operation. Therefore, the interpretation, that $(t)^p$ has the same sign as t and the same magnitude as $|t|^p$ is adopted by using the following operator:

$$(t)^p = \text{sign}(t)|t|^p. \tag{3}$$

To produce only convex shapes, the values for n and e would be bounded: $0 < \{n, e\} < 2$. To prevent numerical overflow and difficulties with singularities, it is advisable to use a further bound: $0.1 < \{n, e\} < 1.9$. The variety of particle shapes, which can be modelled using the superellipsoid equation is plotted in Figure 1.

The variables n and e are varied between 0.2 and 2.0, whereas the bounds a, b and c are kept constant. One can see that a variety of shapes including a sphere, rounded cube, circular or rectangular cylinder, octahedra up to even some star-shaped objects can be generated.

The volume of a superellipsoid can be computed from [40]

$$V = 2 a b c n e B\left(\frac{n}{2} + 1, n\right) B\left(\frac{e}{2}, \frac{e}{2}\right). \tag{4}$$

The term $B(x, y)$ is the beta function, which is related to the gamma function:

$$B(x, y) = 2 \int_0^{\pi/2} \sin^{2x-1} \phi \cos^{2y-1} \phi d\phi = \frac{\Gamma(x) \Gamma(y)}{\Gamma(x+y)}. \tag{5}$$

The volume of some exemplary superellipsoids is given in Table 1.

Table 1: Volume of some exemplary superellipsoids.

e, n	0	0.2	0.5	0.7	1.0	2.0
V	$8abc$	$7.657abc$	$6.482abc$	$5.538abc$	$4.189abc$	$1.333abc$

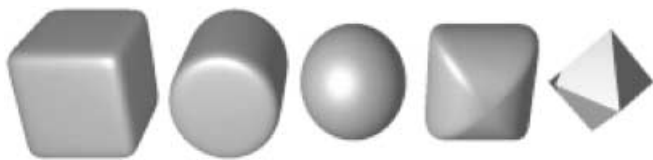


Fig. 1: Examples of superellipsoids with parameters: $e = 0.2; 1.0; 1.0; 0.2; 2.0$ and $n = 0.2; 0.2; 1.0; 1.0; 2.0$. (left to right). $a = b = c = 1.0$.



Fig. 2: Form of rounded cubes used for computation $e = n = 0.2; 0.5; 0.7$ (left to right). In the examples the dimensions are $a = b = c = 0.3 \mu\text{m}$ and the numbers of triangular patches are 1448, 1448, 1400.

For the exemplary computation, in the following section the rounded cube shapes depicted in Figure 2 will be used. The parameters n and e are 0.2, 0.5 and 0.7 such that cubes with different roundedness result.

3 Null-field Method with Discrete Sources

In this section we outline the basics of the *null-field method with discrete sources*[28]. Let us consider a three-dimensional space D consisting of the union of a closed surface S , its interior D_i and its exterior D_s . We denote by k_t the wavenumber in the domain D_t , where $k_t = k \sqrt{\epsilon_t \mu_t}$, $k = \omega/c$ and $t = s, i$.

The transmission boundary-value problem can be formulated as follows. Let $\mathbf{E}_0, \mathbf{H}_0$ be an entire solution to the Maxwell equations representing an incident electromagnetic field. Find the vector fields, $\mathbf{E}_s, \mathbf{H}_s \in C^1(D_s) \cap C(\overline{D_s})$ and $\mathbf{E}_i, \mathbf{H}_i \in C^1(D_i) \cap C(\overline{D_i})$ satisfying the Maxwell's equations

$$\begin{aligned} \nabla \times \mathbf{E}_t &= jk_t \mu_t \mathbf{H}_t, \\ \nabla \times \mathbf{H}_t &= -jk_t \epsilon_t \mathbf{E}_t, \end{aligned} \tag{6}$$

in D_t , where $t = s, i$, and two boundary conditions:

$$\begin{aligned} \mathbf{n} \times \mathbf{E}_i - \mathbf{n} \times \mathbf{E}_s &= \mathbf{n} \times \mathbf{E}_0, \\ \mathbf{n} \times \mathbf{H}_i - \mathbf{n} \times \mathbf{H}_s &= \mathbf{n} \times \mathbf{H}_0, \end{aligned} \tag{7}$$

on S . In addition, the scattered field $\mathbf{E}_s, \mathbf{H}_s$ must satisfy the Silver-Müller radiation condition uniformly for all directions \mathbf{x}/x . It is known that the transmission boundary-value problem possesses a unique solution[41].

For solving the transmission boundary-value problem in the framework of the null-field method with discrete sources, the scattering object is replaced by a set of surface current densities \mathbf{e} and \mathbf{h} , so that in the exterior domain the sources and fields are exactly the same as those existing in the original scattering problem. The entire analysis can conveniently be broken down into the following three steps:

(I) A set of integral equations for the surface current densities \mathbf{e} and \mathbf{h} is derived for a variety of discrete

sources. Physically, the set of integral equations in question guarantees the null-field condition within D_i . It is noted that localized and distributed vector spherical functions, magnetic and electric dipoles or vector Mie potentials can be used as discrete sources. Essentially, the null-field method with discrete sources consists in the projection relations:

$$\int_S \left[(\mathbf{e} - \mathbf{e}_0) \cdot \Psi_\nu^3 + j \sqrt{\frac{\mu_s}{\epsilon_s}} (\mathbf{h} - \mathbf{h}_0) \cdot \Phi_\nu^3 \right] dS = 0$$

$$\int_S \left[(\mathbf{e} - \mathbf{e}_0) \cdot \Phi_\nu^3 + j \sqrt{\frac{\mu_s}{\epsilon_s}} (\mathbf{h} - \mathbf{h}_0) \cdot \Psi_\nu^3 \right] dS = 0, \quad \nu = 1, 2, \dots \quad (8)$$

where $\mathbf{e}_0 = \mathbf{n} \times \mathbf{E}_0$ and $\mathbf{h}_0 = \mathbf{n} \times \mathbf{H}_0$ are the tangential components of the incident electric and magnetic fields. The set $\{\Psi_\nu^3, \Phi_\nu^3\}_{\nu=1,2,\dots}$ consists of radiating solutions to Maxwell equations and depends on the system of discrete sources which is used for imposing the null-field condition. Actually, this set together with the set of regular solutions to Maxwell equations $\{\Psi_\nu^1, \Phi_\nu^1\}_{\nu=1,2,\dots}$ stands for

– localized vector spherical functions $\{\mathbf{M}_{mn}^{1,3}, \mathbf{N}_{mn}^{1,3}\}_{m \in \mathbf{Z}, n \geq \max(1, |m|)}$:

$$\mathbf{M}_{mn}^{1,3}(k\mathbf{x}) = \sqrt{D_{mn}} z_n(kr) \left[jm \frac{P_n^{|m|}(\cos\theta)}{\sin\theta} \mathbf{e}_\theta - \frac{dP_n^{|m|}(\cos\theta)}{d\theta} \mathbf{e}_\varphi \right] e^{jm\varphi},$$

$$\mathbf{N}_{mn}^{1,3}(k\mathbf{x}) = \sqrt{D_{mn}} \left\{ n(n+1) \frac{z_n(kr)}{kr} P_n^{|m|}(\cos\theta) e^{jm\varphi} \mathbf{e}_r + \frac{[krz_n(kr)]'}{kr} \left[\frac{dP_n^{|m|}(\cos\theta)}{d\theta} \mathbf{e}_\theta + jm \frac{P_n^{|m|}(\cos\theta)}{\sin\theta} \mathbf{e}_\varphi \right] \right\} e^{jm\varphi}, \quad (9)$$

where $(\mathbf{e}_r, \mathbf{e}_\theta, \mathbf{e}_\varphi)$ are the unit vectors in spherical coordinates, z_n designates the spherical Bessel functions j_n or the spherical Hankel functions of the first kind h_n^1 , $P_n^{|m|}$ denotes the associated Legendre polynomial of order n and m , and D_{mn} is a normalization constant given by

$$D_{mn} = \frac{2n+1}{4n(n+1)} \cdot \frac{(n-|m|)!}{(n+|m|)!}, \quad (10)$$

– distributed vector spherical functions $\{\mathcal{M}_{mn}^{1,3}, \mathcal{N}_{mn}^{1,3}\}_{m \in \mathbf{Z}, n=1,2,\dots}$:

$$\mathcal{M}_{mn}^{1,3}(k\mathbf{x}) = \mathbf{M}_{m,|m|+l}^{1,3}(k(\mathbf{x} - z_n \mathbf{e}_3)), \quad \mathbf{x} \in \mathbf{R}^3 - \{z_n \mathbf{e}_3\}_{n=1}^\infty,$$

$$\mathcal{N}_{mn}^{1,3}(k\mathbf{x}) = \mathbf{N}_{m,|m|+l}^{1,3}(k(\mathbf{x} - z_n \mathbf{e}_3)), \quad \mathbf{x} \in \mathbf{R}^3 - \{z_n \mathbf{e}_3\}_{n=1}^\infty, \quad (11)$$

where $m \in \mathbf{Z}, n = 1, 2, \dots, l = 1$ if $m = 0$ and $l = 0$ if $m \neq 0$, and $\{z_n\}_{n=1}^\infty$ is a set of points located on a segment Γ_z of the z -axis,

– magnetic and electric dipoles $\{\mathcal{M}_{ni}^{1,3}, \mathcal{N}_{ni}^{1,3}\}_{n=1,2,\dots,i=1,2}$:

$$\mathcal{M}_{ni}^{1,3}(k\mathbf{x}) = \mathbf{m}(\mathbf{x}_n^\pm, \mathbf{x}, \tau_{ni}^\pm), \quad \mathbf{x} \in \mathbf{R}^3 - \{\mathbf{x}_n^\pm\}_{n=1}^\infty,$$

$$\mathcal{N}_{ni}^{1,3}(k\mathbf{x}) = \mathbf{n}(\mathbf{x}_n^\pm, \mathbf{x}, \tau_{ni}^\pm), \quad \mathbf{x} \in \mathbf{R}^3 - \{\mathbf{x}_n^\pm\}_{n=1}^\infty, \quad (12)$$

where $n = 1, 2, \dots, i = 1, 2, \tau_{n1}$ and τ_{n2} are two tangential linear independent unit vectors at the point \mathbf{x}_n ,

$$\mathbf{m}(\mathbf{x}, \mathbf{y}, \mathbf{a}) = \frac{1}{k^2} \mathbf{a}(\mathbf{x}) \times \nabla_y g(\mathbf{x}, \mathbf{y}, k), \quad \mathbf{n}(\mathbf{x}, \mathbf{y}, \mathbf{a}) = \frac{1}{k} \nabla_y \times \mathbf{m}(\mathbf{x}, \mathbf{y}, \mathbf{a}), \quad \mathbf{x} \neq \mathbf{y}, \quad (13)$$

and the sequence $\{\mathbf{x}_n^-\}_{n=1}^\infty$ is dense on a smooth surface S^- enclosed in D_i , while the sequence $\{\mathbf{x}_n^+\}_{n=1}^\infty$ is dense on a smooth surface S^+ enclosing D_i , or finally for the set of – vector Mie-potentials $\{\mathcal{M}_n^{1,3}, \mathcal{N}_n^{1,3}\}_{n=1,2,\dots}$:

$$\mathcal{M}_n^{1,3}(k\mathbf{x}) = \frac{1}{k} \nabla \times (\varphi_n^\pm(\mathbf{x}) \mathbf{x}), \quad \mathbf{x} \in \mathbf{R}^3 - \{\mathbf{x}_n^\pm\}_{n=1}^\infty,$$

$$\mathcal{N}_n^{1,3}(k\mathbf{x}) = \frac{1}{k} \nabla \times \mathcal{M}_n^{1,3}(k\mathbf{x}), \quad \mathbf{x} \in \mathbf{R}^3 - \{\mathbf{x}_n^\pm\}_{n=1}^\infty, \quad (14)$$

where the Green functions

$$\varphi_n^\pm(\mathbf{x}) = g(\mathbf{x}_n^\pm, \mathbf{x}, k), \quad n = 1, 2, \dots$$

have singularities $\{\mathbf{x}_n^-\}_{n=1}^\infty$ and $\{\mathbf{x}_n^+\}_{n=1}^\infty$ distributed on the auxiliary surfaces S^- and S^+ , respectively. By convention, when we refer to the null-field Eqs. (8) we implicitly refer to all equivalent forms of these equations.

(II) The surface current densities are approximated by fields of discrete sources. In this context let \mathbf{e} and \mathbf{h} solve the null-field Eqs. (8) and assume that the system $\{\mathbf{n} \times \Psi_\mu^1, \mathbf{n} \times \Phi_\mu^1\}_{\mu=1}^\infty$ form a Schauder basis in $\mathcal{L}_{\tan}^2(S)$. Then there exists a sequence $\{a_\mu, b_\mu\}_{\mu=1}^\infty$ such that

$$\mathbf{e}(\mathbf{y}) = \sum_{\mu=1}^\infty a_\mu \mathbf{n} \times \Psi_\mu^1(k, \mathbf{y}) + b_\mu \mathbf{n} \times \Phi_\mu^1(k, \mathbf{y}), \quad \mathbf{y} \in S,$$

$$\mathbf{h}(\mathbf{y}) = -j \sqrt{\frac{\epsilon_i}{\mu_i}} \sum_{\mu=1}^\infty a_\mu \mathbf{n} \times \Phi_\mu^1(k, \mathbf{y}) + b_\mu \mathbf{n} \times \Psi_\mu^1(k, \mathbf{y}), \quad \mathbf{y} \in S. \quad (15)$$

We recall that a system $\{\psi_i\}_{i=1}^\infty$ is called a Schauder basis of a Banach space X if any element $u \in X$ can be uniquely represented as $u = \sum_{i=1}^\infty \alpha_i \psi_i$, where the convergence of the series is in the norm of X . It is noted that in the case of localized vector spherical functions the notion of Schauder basis is closely connected with the Rayleigh hypothesis. This hypothesis says that the series

representation of the scattered field in terms of radiating localized vector spherical functions, which uniformly converges outside the circumscribing sphere, also converges on S .

(III) Once the surface current densities have been determined, the scattered field outside the circumscribing sphere is obtained by using the representation theorem. We obtain the series representation

$$\mathbf{E}_s(\mathbf{x}) = \sum_{\nu=1}^{\infty} f_{\nu} \mathbf{M}_{\bar{\nu}}^3(k_s \mathbf{x}) + g_{\nu} \mathbf{N}_{\bar{\nu}}^3(k_s \mathbf{x}), \quad (16)$$

where

$$\begin{aligned} f_{\nu} &= \frac{jk_s^2}{\pi} \int_S \left[\mathbf{e}(\mathbf{y}) \cdot \mathbf{N}_{\bar{\nu}}^1(k_s \mathbf{y}) + j \sqrt{\frac{\mu_s}{\epsilon_s}} \mathbf{h}(\mathbf{y}) \cdot \mathbf{M}_{\bar{\nu}}^1(k_s \mathbf{y}) \right] dS(\mathbf{y}), \\ g_{\nu} &= \frac{jk_s^2}{\pi} \int_S \left[\mathbf{e}(\mathbf{y}) \cdot \mathbf{M}_{\bar{\nu}}^1(k_s \mathbf{y}) + j \sqrt{\frac{\mu_s}{\epsilon_s}} \mathbf{h}(\mathbf{y}) \cdot \mathbf{N}_{\bar{\nu}}^1(k_s \mathbf{y}) \right] dS(\mathbf{y}). \end{aligned} \quad (17)$$

Here, $\bar{\nu}$ is a complex index incorporating $-m$ and n , i.e. $\bar{\nu} = (-m, n)$.

3.1 T-matrix Computation

Now, for deriving the T-matrix let us assume that the incident field can be expressed inside a finite region containing S as a series of regular vector spherical functions

$$\begin{aligned} \mathbf{E}_0(\mathbf{x}) &= \sum_{\nu=1}^{\infty} a_{\nu}^0 \mathbf{M}_{\nu}^1(k_s \mathbf{x}) + b_{\nu}^0 \mathbf{N}_{\nu}^1(k_s \mathbf{x}), \\ \mathbf{H}_0(\mathbf{x}) &= -j \sqrt{\frac{\epsilon_s}{\mu_s}} \sum_{\nu=1}^{\infty} a_{\nu}^0 \mathbf{N}_{\nu}^1(k_s \mathbf{x}) + b_{\nu}^0 \mathbf{M}_{\nu}^1(k_s \mathbf{x}). \end{aligned} \quad (18)$$

Then, using Eqs. (8)–(18) we see that the relation between the scattered and the incident field coefficients is linear and is given by a transition matrix \mathbf{T} as follows:

$$\begin{bmatrix} f_{\nu} \\ g_{\nu} \end{bmatrix} = \mathbf{T} \begin{bmatrix} a_{\nu}^0 \\ b_{\nu}^0 \end{bmatrix} \quad (19)$$

where

$$\mathbf{T} = \mathbf{B} \mathbf{A}^{-1} \mathbf{A}_0, \quad (20)$$

and \mathbf{A} , \mathbf{B} and \mathbf{A}_0 are block matrices written in general as

$$\mathbf{X} = \begin{bmatrix} X_{\nu\mu}^{11} & X_{\nu\mu}^{12} \\ X_{\nu\mu}^{21} & X_{\nu\mu}^{22} \end{bmatrix}, \quad \nu, \mu = 1, 2, \dots, \quad (21)$$

with \mathbf{X} standing for \mathbf{A} , \mathbf{B} and \mathbf{A}_0 . Explicit expressions for the elements of these matrices are given in the Appendix. It is noted that the exact infinite T-matrix is independent of the expansion systems used on S . However, the approximate truncated matrix, computed according to

$$\mathbf{T}_N = \mathbf{B}_N \mathbf{A}_N^{-1} \mathbf{A}_{0N} \quad (22)$$

does contain such a dependence.

Energy characteristics in the far field are computed from the far-field pattern \mathbf{E}_{s0}^N for a unit amplitude incident electric field for p- or s-polarization. The angle-dependent intensity function plotted in the simulation section is the normalized differential scattering cross-section (DSCS):

$$\frac{\sigma_d}{\pi a^2} = \frac{|k_s \mathbf{E}_{s0}^N|^2}{\pi |k_s a|^2}. \quad (23)$$

To compute numerically orientation-averaged scattering, three integrals with respect to the three Euler α, β, γ angles have to be computed. Thus the value of interest $f(\alpha, \beta, \gamma)$ is integrated over all directions and polarization of the incident plane wave. The numerical procedure used to do this is based on a stepwise procedure:

$$\begin{aligned} \int_0^{2\pi} \int_0^{\pi} \int_0^{2\pi} f(\alpha, \beta, \gamma) d\alpha \sin \beta d\beta d\gamma &\approx \sum_{n_{\alpha}=1}^{N_{\alpha}} \sum_{n_{\beta}=1}^{N_{\beta}} \sum_{n_{\gamma}=1}^{N_{\gamma}} \\ &\times f(\alpha, \beta, \gamma) \sin(n_{\beta}\pi/N_{\beta}) \frac{n_{\alpha} 2\pi n_{\beta} \pi n_{\gamma} 2\pi}{N_{\alpha} N_{\beta} N_{\gamma}}. \end{aligned} \quad (24)$$

The triple integral is converted to three summations. The angle α is digitized for N_{α} steps in the range $(0, 2\pi)$, angle β is digitized for N_{β} steps in the range $(0, \pi)$, and angle γ is digitized for N_{γ} steps in the range $(0, 2\pi)$.

4 Mesh Generation

Implicit surfaces are commonly used for modelling purposes in numerous scientific applications, including CAD system and computer graphics. Therefore, there are various interests in constructing a polyhedral representation of implicit surfaces [42]. In our case, the representation in a triangular patch model should allow first a correct calculation of surface integrals and second a graphical visualization of the particle. Different methods are available to create a geometric surface mesh.

To generate the superellipsoid shape for our light scattering simulations we use the *HyperFun* software

tool [43, 44] which is a program supporting high-level language functional representations in computer graphics. Function representation is a generalization of traditional implicit surfaces and constructive solid geometry which allows the construction of complex shapes such as isosurfaces of real-valued functions composed of functionally defined primitives and operations [45]. The *HyperFun* polygonizer used for surface mesh generation generates VRML output of a triangular patch model. *HyperFun* generates a sufficiently regular mesh which, although intended for computer graphics, is very well suited for our application, as we found.

An example of gridding is shown with the rounded cubes given in Figure 2. In these examples the dimensions are $a = b = c = 0.3 \mu\text{m}$ and the numbers of triangular patches are 1448, 1448, 1400.

In the standard method to compute surface integrals, the parametric equation is used and therefore an equivalent integral in planar coordinates has to be evaluated. Hence, partial derivatives of x, y, z with respect to the parametrization (in our case parameters ϑ, φ) are needed, which may not be available analytically. If the partial derivatives are not available, a numerical method via finite differences may be used.

We use an alternative approach based on a modified centroid quadrature that does not use the partial derivatives. This modified centroid quadrature has been proposed and investigated by *Georg and Tauch* [46]. The surface integrals to be computed are approximated by

$$\int_S f dS \approx \sum_i f(v_{i,c}) \text{area}[v_{i,1}, v_{i,2}, v_{i,3}], \quad (25)$$

where, $v_{i,1}, v_{i,2}, v_{i,3}$ are the vertices spanning a triangle and point $v_{i,c}$ denotes the centre of mass of the triangle $[v_{i,1}, v_{i,2}, v_{i,3}]$ given by

$$v_{i,c} = \frac{1}{3} \sum_{j=1}^3 v_{i,j}. \quad (26)$$

Thus, the integral over each triangle is approximated by multiplying the value of the integrand at the centroid by the triangle area.

5 Numerical Simulations

5.1 Program Validation

The computer program based on the DSM theory was checked using various internal checks such as computing scattering by a shifted particle and comparing the result with scattering by the original particle.

Next, the program was validated by comparing it with other programs. We used the T-Matrix programs t1 included with the book by *Barber and Hill* [7]. The first result is for a spheroid with dimensions of $a = b = 500 \text{ nm}$ and $c = 700 \text{ nm}$. Practically no difference was found, as can be seen by the normalized DSCS for p- and s-polarization plotted in Figure 3. The T-Matrix result is shifted with respect to the DSM result because *Barber and Hill* apply a different normalization in the differential scattering cross section (DSCS) computed. To check the routine for orientation averaging, the program t5 of *Barber and Hill* [7] is used to compute a reference result of the orientation averaged DSCS for the same spheroid. The results of both computations are plotted in Figure 4 and there is perfect agreement between the

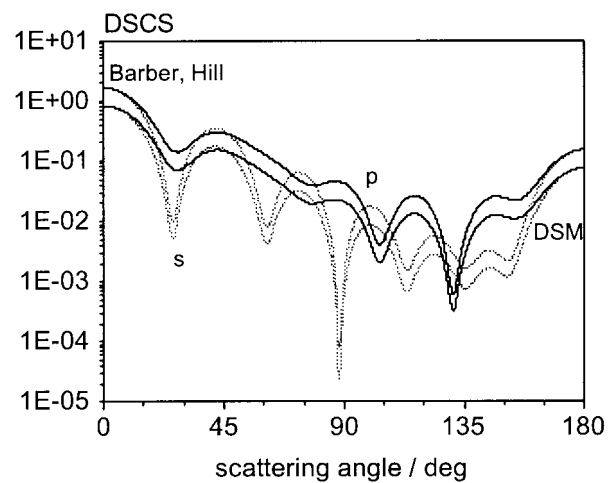


Fig. 3: Differential scattering cross-section of spheroid $a = b = 500 \text{ nm}$, $c = 700 \text{ nm}$, 10725 faces, $N_{\text{max}} = 16$, $M_{\text{max}} = 15$, $M = 1.5$, $\lambda = 628.31 \text{ nm}$.

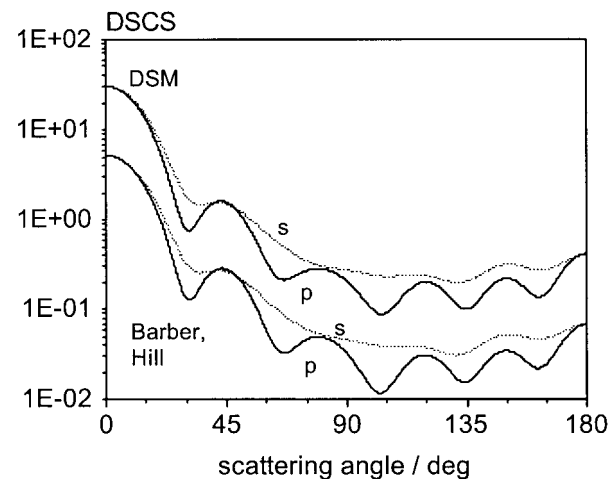


Fig. 4: Orientation-averaged differential scattering cross-section of spheroid $a = b = 500 \text{ nm}$, $c = 700 \text{ nm}$, 10725 faces, 1000 orientations, $N_{\text{max}} = 16$, $M_{\text{max}} = 15$, $M = 1.5$, $\lambda = 628.31 \text{ nm}$.

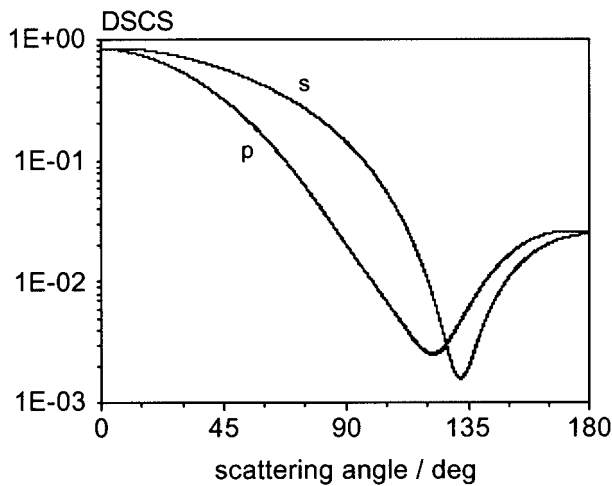


Fig. 5: Differential scattering cross-section of ellipsoid $a = 150$, $b = 200$, $c = 300$ nm, 11656 faces, 64×64 , $M = 1.5$, $\lambda = 628.31$ nm, $pol = 45^\circ$

results computed by the DSM program and the t5 program.

As another example of program validation, scattering by an ellipsoid with dimensions $a = 150$, $b = 200$ and $c = 300$ nm is presented in Figure 5. The comparative result of the DSCS was computed with another implementation of the same theory [34]. As can be seen, there is perfect agreement between the two sets of results.

To present a final example of program validation for non-axisymmetric particles, the 3D-Multiple Multipole Program (MMP) of *Hafner and Bomholt* [47] was used for computation of a scattering result of a rounded cube for comparison with. This method is based on an expansion of the internal and the scattered field into so-called multipoles. A generalized point matching method is used to fulfil the boundary conditions on the surface of the scattering particle and to compute the coefficients of the expansion functions. In the example given we used spherical vector wavefunctions for field expansion. The FORTRAN code is available with the MMP book and this code was modified such that a triangular surface patch model of the scattering particle could be read into the program to be used for the point matching procedure. As mirror symmetry can be accounted for in the MMP program, only an eighth of the surface of the rounded cube has to be used for triangulation into a triangular surface patch model. In the example presented, this surface was covered by 1435 faces. The rounded cube was generated by the superellipsoid equation with the parameters $e = n = 0.2$ and $a = b = c = 1.0$ μm . The computational results of the differential scattering cross-section are plotted in Figures 6 and 7. Apart from some different normalization of the DSCS there is almost perfect agreement between the MMP and DSM results.

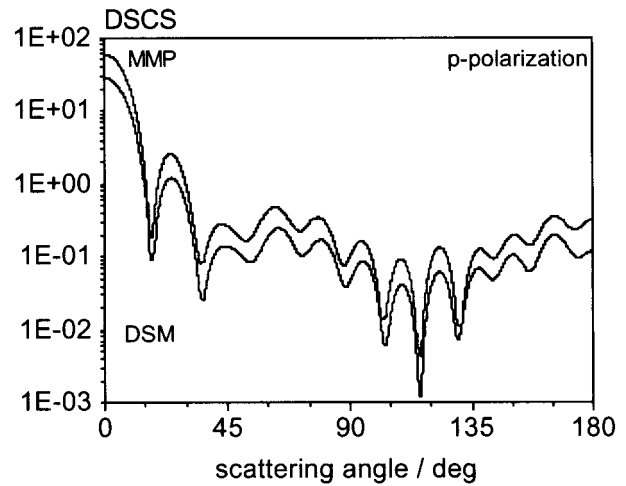


Fig. 6: Differential scattering cross-section (p-polarization) of rounded cube with parameters $e = n = 0.2$, $a = b = c = 1000$ nm, $N_{\max} = 20$, $M_{\max} = 18$, $M = 1.5$, $\lambda = 628.31$ nm, DSM: 14648 faces; MMP 1/8 of cube with 1435 faces.

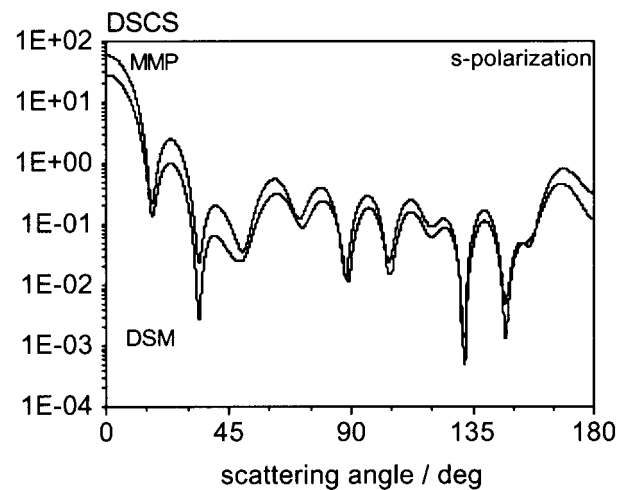


Fig. 7: Differential scattering cross-section (s-polarization) of rounded cube with parameters $e = n = 0.2$, $a = b = c = 1000$ nm, $N_{\max} = 20$, $M_{\max} = 18$, $M = 1.5$, $\lambda = 628.31$ nm, DSM: 14648 faces; MMP 1/8 of cube with 1435 faces.

5.2 Convergence

A profound convergence test is an important step in program testing. Two kinds of convergence checks have to be made: (a) versus the number of triangular faces of the particles, corresponding to the number of integration elements and, (b) versus the number of localized spherical vector wavefunctions used for field expansion. Figure 8 shows an exemplary result for a convergence test versus the number of integration elements (faces) for a rounded cube with parameters $a = 300$ nm, $n = e = 0.2$ and refractive index $M = 1.5$. By comparing the curves it can be seen that convergence is easily reached and from further investigation we conclude that convergence

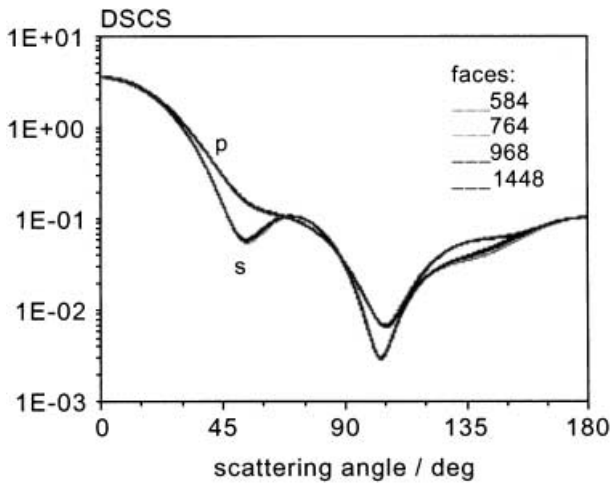


Fig. 8: DSCS computed for convergence test versus number of integration points (faces) for a cube. $a = b = c = 300$ nm, $n = e = 0.2$, $N_{\max} = 10$, $M_{\max} = 7$, $M = 1.5$; $\lambda = 628.31$ nm.

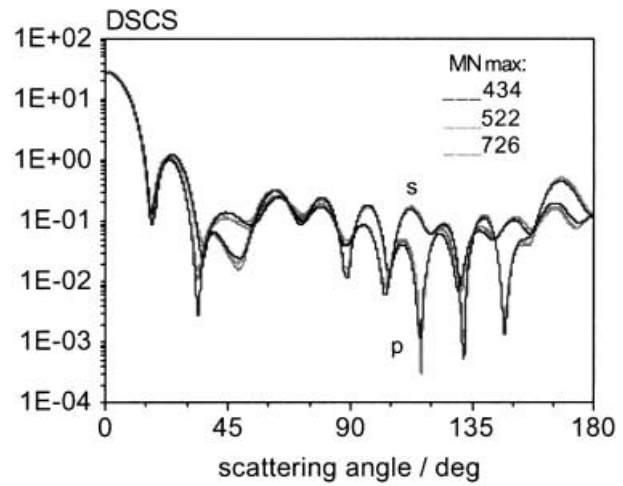


Fig. 9: DSCS computed for convergence test versus number of expansion functions MN_{\max} for a cube $a = b = c = 1000$ nm, $n = e = 0.5$, 14648 faces, $M = 1.5$, $\lambda = 628.31$ nm.

versus the number of integration elements seems to be mainly uncritical and can easily be achieved. Of more importance is a convergence check versus the number of expansion functions. This number depends on the maximum value of the indices n and m (N_{\max} and M_{\max}) of the spherical vector wavefunctions $\mathbf{M}_{\vec{r}}$ and $\mathbf{N}_{\vec{r}}$. This number of expansion functions MN_{\max} is given by

$$MN_{\max} = N_{\max} + M_{\max}(2N_{\max} - M_{\max} + 1). \quad (27)$$

This corresponds to a size of the transition matrix given by $\mathbf{T}(2MN_{\max}, 2MN_{\max})$. Various convergence checks were applied to test the program for different shapes of scatterers. An exemplary result of such a convergence test is given in Figure 9, where the differential scattering cross-section is plotted for a cube. The values of the parameters N_{\max} and M_{\max} used in the simulation and the resulting corresponding number of expansion functions MN_{\max} are summarized in Table 2.

Table 2: Number of expansion functions.

N_{\max}	M_{\max}	MN_{\max}
20	18	434
22	20	522
25	25	726

5.2.1 Scattering by Rounded Cube

In this section, some sample results of single scattering by the superellipsoids pictured in Figure 2 are presented. Figures 10 and 11 give the differential scattering cross-sections of a cube with dimensions $a = b = c = 1.5 \mu\text{m}$ and different values of the two roundedness parameters. The first figure gives p-polarization and the second s-polarization.

Scattering by even larger rounded cubes is plotted in Figures 12 and 13, which give the differential scattering cross-section of a cube with dimensions and different values of the two roundedness parameters. The influence

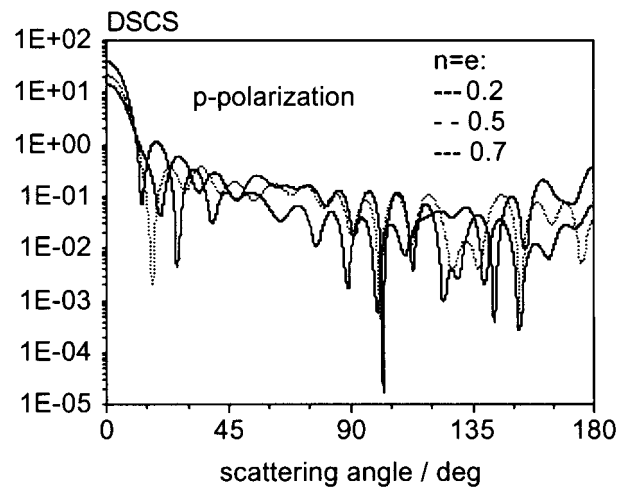


Fig. 10: Differential scattering cross-section (p-polarization) of rounded cube with different values of e and n , $a = b = c = 1500$ nm, $N_{\max} = 30$, $M_{\max} = 28$, 33464 faces, $M = 1.5$, $\lambda = 628.31$ nm.

of roundedness is especially seen in p-polarization at a scattering angle of $45 - 90^\circ$.

Just a single exemplary scattering result for orientation-averaged scattering by a rounded cube with roundedness parameters $e, n = 0.5$ is given in Figure 14. The p- and s-polarization results almost become indistinguishable and

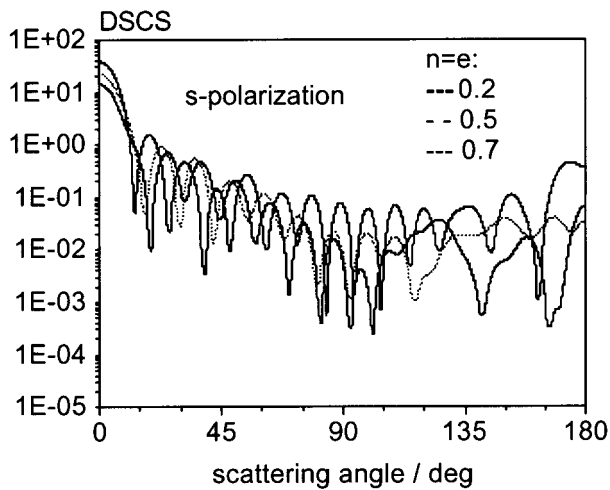


Fig. 11: Differential scattering cross-section (s-polarization) of rounded cube with different values of e and n , $a = b = c = 1500$ nm, $N_{\max} = 30$, $M_{\max} = 28$, 33464 faces, $M = 1.5$, $\lambda = 628.31$ nm.

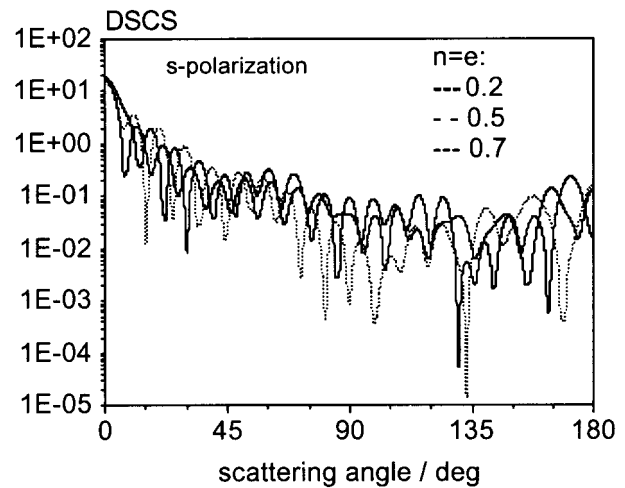


Fig. 13: Differential scattering cross-section (s-polarization) of rounded cube with different values of e and n , $a = b = c = 2000$ nm, $N_{\max} = 39$, $M_{\max} = 38$, 76220 faces, $M = 1.5$, $\lambda = 628.31$ nm.

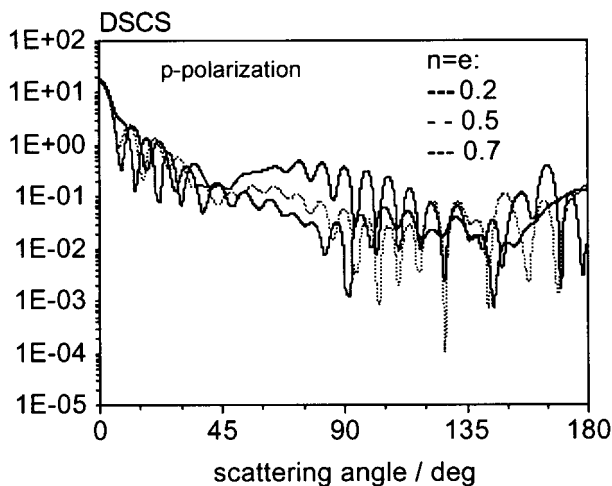


Fig. 12: Differential scattering cross-section (p-polarization) of rounded cube with different values of e and n , $a = b = c = 2000$ nm, $N_{\max} = 39$, $M_{\max} = 38$, 76220 faces, $M = 1.5$, $\lambda = 628.31$ nm.

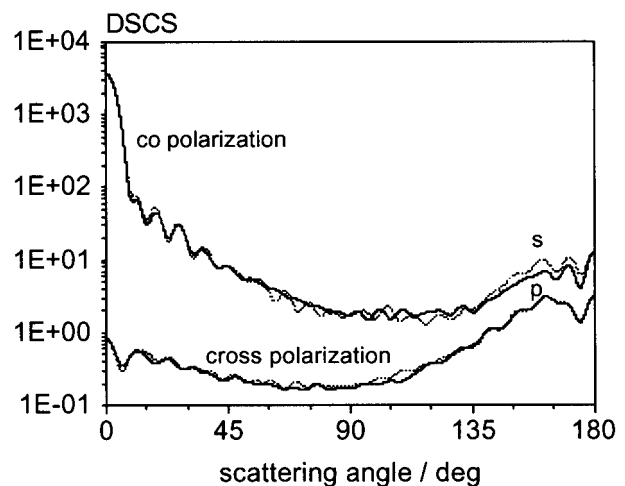


Fig. 14: Orientation averaged differential scattering cross-section of rounded cube with $e = n = 0.5$, $a = b = c = 2000$ nm, $N_{\max} = 39$, $M_{\max} = 38$, 76220 faces, 2744 orientation, $M = 1.5$, $\lambda = 628.31$ nm.

the angular variation in the DSCS is much smoother than that for the same particle in a fixed orientation.

5.2.2 Scattering by Realistically Shaped Particles

To demonstrate that scattering by an arbitrarily shaped particle is also possible with the program developed, the shape of asteroid KY26 was used. Its shape is available as a triangular surface patch model in the wavefront format on the Internet [48]. There are 4092 faces in the data file and the dimensions of the 0.030 km asteroid were scaled down by a factor of 100 $\mu\text{m}/\text{km}$ such that a particle with a range of 2.92 μm in x , 2.64 μm in y and 2.77 μm in z resulted. Three different views of this KY26-shaped

particle are given in Figure 15. The number of triangular faces was increased to 16368 using a one-to-four triangular subdivision scheme. In Figure 16 the differential scattering cross-section is plotted. As orientation, the orientation given in the original data file was used with z being the direction of the incident plane wave. In Figure 17 the orientation-averaged differential scattering cross-section is given. It can be seen that the angular variation in the DSCS is smoother than that computed for the same particle in a fixed orientation.

To demonstrate that scattering from realistically shaped particles can be computed, a number of photographs of a pebble from different views were used to reconstruct a realistic particle shape. Similarly, electron microscopy

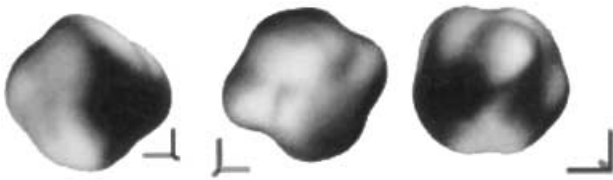


Fig. 15: Three views of KY26-shaped particle scaled down by 100 μm/km.



Fig. 18: Three views of “realistically” shaped particle.

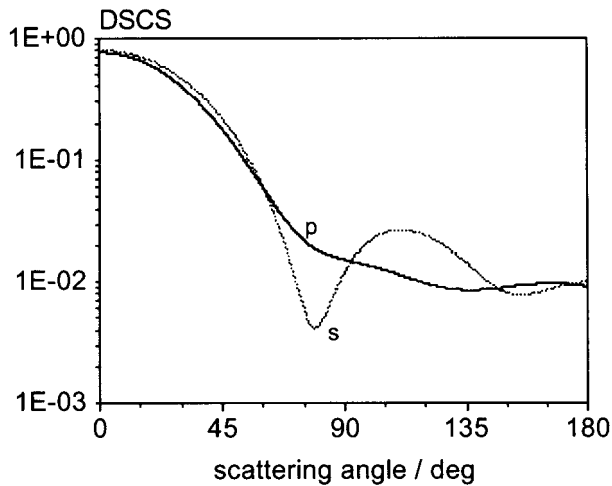


Fig. 16: Differential scattering cross-section of KY26-shaped particle, $N_{\max} = 10$, $M_{\max} = 7$, 4092 faces, $M = 1.5$, $\lambda = 628.31$ nm.

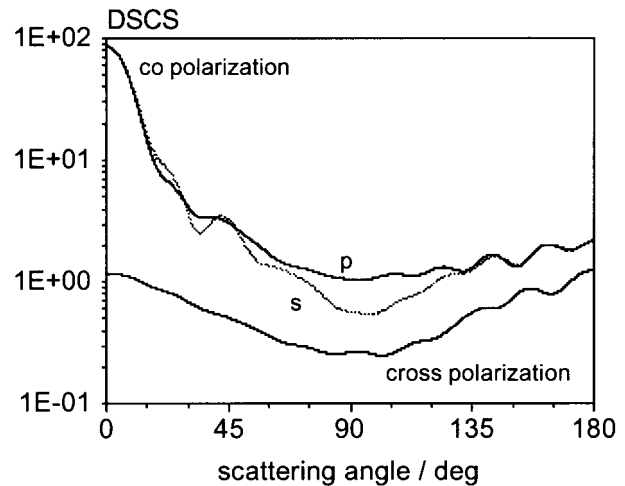


Fig. 19: Orientation-averaged differential scattering cross-section of “real” shaped particle, 1728 orientations, $N_{\max} = 20$, $M_{\max} = 17$, 28032 faces, $M = 1.50$, $\lambda = 628.31$ nm.

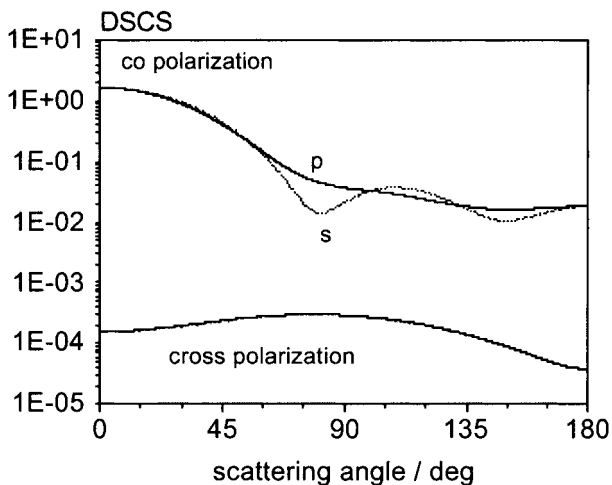


Fig. 17: Orientation-averaged differential scattering cross-section of KY26-shaped particle, 1000 orientations, $N_{\max} = 10$, $M_{\max} = 7$, 4092 faces, $M = 1.5$, $\lambda = 628.31$ nm.

from different views of a small particle could be used to reconstruct its 3D shape. The geometry of the pebble was reconstructed from an image sequence of apparent contour profiles from 20 different viewpoints taken by an electronic camera [49].

Three views of the reconstructed realistically shaped particle are shown in Figure 18. The dimensions of the particle were scaled such that its size in x is 2.176 μm in y

is 1.585 μm and in z is 1.856 μm. The shape of the particle was triangulated with 27745 faces. In Figure 19 the orientation-averaged differential scattering cross-section of this particle is plotted.

To generate an arbitrarily shaped particle with a different amount of surface roughness, the DOS program Pov-RockGen [50] was used. The dimensions of the particles generated are such that its overall size in x is 2.026 μm, in y is 2.026 μm and in z is 1.969 μm. The parameters for generating the smooth particle are depth=4 and smoothness=2.0 and the parameters for generating the rough particle are depth=4 and smoothness=1.5. Originally 5120 surface triangles were generated. These were increased to 20480 by a one-to-four triangular subdivision scheme.

The two different kinds of particle shapes generated and used for scattering computations are shown in Figure 20 and the orientation-averaged computation results are plotted in Figure 21. With the smooth particle, oscillations in the scattering diagram are more pronounced. With the rougher particle, the amount of cross-polarization is, of course, increased.



Fig. 20: Shape of smooth (left) and rough (right) particles.

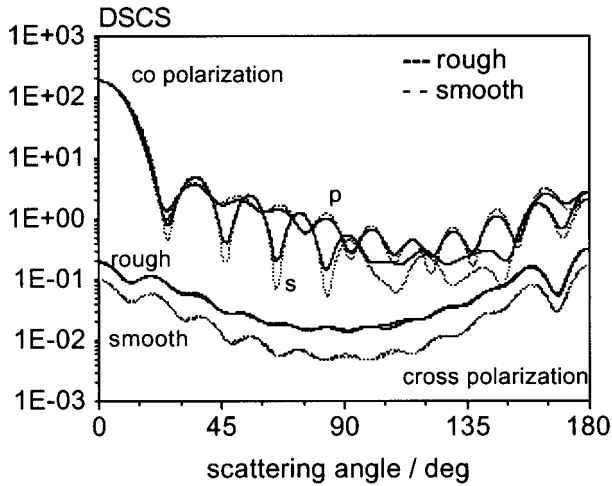


Fig. 21: Orientation-averaged differential scattering cross-section of smooth and rough particles, 1728 orientations, $N_{\max} = 20$, $M_{\max} = 17$, 20480 faces, $M = 1.5$, $\lambda = 628.31$ nm.

6 Conclusions

An efficient way for computing scattering by non-axisymmetric particles in the framework of the *null-field method with discrete sources* has been presented. The superellipsoid has been introduced to represent a wide range of realistic particle shapes. Additionally, reading a triangular surface patch model of a scattering particle has been implemented in the computational procedure.

Numerical experiments have been performed for superellipsoids representing a rounded dielectric cube and some realistically shaped particles. It has been demonstrated that this method is very well suited to compute the T-matrix for non-axisymmetric particles with an overall dimension of $4 \mu\text{m}$ with a desktop computer. A Windows 9X program including graphical user interface for computing scattering by a superellipsoid is available from our web site [51].

The program has mainly been developed to investigate the effect of particle shape with various kind of methods and instruments in optical particle characterization such as intensity-based optical particle counters, intensity ratioing technique, visibility technique, phase Doppler anemometry, diffraction type of instruments, static light scattering, etc.

7 Appendix

The block elements of matrices \mathbf{A} , \mathbf{B} and \mathbf{A}_0 are given by

$$\begin{aligned} A_{\nu\mu}^{11} &= \int_S \left[(n \times \Psi_\mu^1) \cdot \Psi_\nu^3 + M(n \times \Phi_\mu^1) \cdot \Phi_\nu^3 \right] dS, \\ A_{\nu\mu}^{12} &= \int_S \left[(n \times \Phi_\mu^1) \cdot \Psi_\nu^3 + M(n \times \Psi_\mu^1) \cdot \Phi_\nu^3 \right] dS, \\ A_{\nu\mu}^{21} &= \int_S \left[(n \times \Psi_\mu^1) \cdot \Phi_\nu^3 + M(n \times \Phi_\mu^1) \cdot \Psi_\nu^3 \right] dS, \\ A_{\nu\mu}^{22} &= \int_S \left[(n \times \Phi_\mu^1) \cdot \Phi_\nu^3 + M(n \times \Psi_\mu^1) \cdot \Psi_\nu^3 \right] dS, \end{aligned} \quad (28)$$

$$\begin{aligned} B_{\nu\mu}^{11} &= \frac{ik^2}{\pi} \int_S \left[(n \times \Psi_\mu^1) \cdot N_\nu^1 + M(n \times \Phi_\mu^1) \cdot M_\mu^1 \right] dS, \\ B_{\nu\mu}^{12} &= \frac{ik^2}{\pi} \int_S \left[(n \times \Phi_\mu^1) \cdot N_\nu^1 + M(n \times \Psi_\mu^1) \cdot M_\mu^1 \right] dS, \\ B_{\nu\mu}^{21} &= \frac{ik^2}{\pi} \int_S \left[(n \times \Psi_\mu^1) \cdot M_\nu^1 + M(n \times \Phi_\mu^1) \cdot N_\mu^1 \right] dS, \\ B_{\nu\mu}^{22} &= \frac{ik^2}{\pi} \int_S \left[(n \times \Phi_\mu^1) \cdot M_\nu^1 + M(n \times \Psi_\mu^1) \cdot N_\mu^1 \right] dS, \end{aligned} \quad (29)$$

$$\begin{aligned} A_{0\nu\mu}^{11} &= \int_S \left[(n \times M_\mu^1) \cdot \Psi_\nu^3 + (n \times N_\mu^1) \cdot \Phi_\nu^3 \right] dS, \\ A_{0\nu\mu}^{12} &= \int_S \left[(n \times N_\mu^1) \cdot \Psi_\nu^3 + (n \times M_\mu^1) \cdot \Phi_\nu^3 \right] dS, \\ A_{0\nu\mu}^{21} &= \int_S \left[(n \times M_\mu^1) \cdot \Phi_\nu^3 + (n \times N_\mu^1) \cdot \Psi_\nu^3 \right] dS, \\ A_{0\nu\mu}^{22} &= \int_S \left[(n \times N_\mu^1) \cdot \Phi_\nu^3 + (n \times M_\mu^1) \cdot \Psi_\nu^3 \right] dS, \end{aligned} \quad (30)$$

respectively. Here, M is the refractive index and is given by $M = \sqrt{\epsilon_i/\epsilon_s}$.

8 Acknowledgement

We acknowledge support of this work by the Deutsche Forschungsgemeinschaft (DFG).

9 Symbols and Abbreviations

a, b, c	bounds in x, y, z of the superellipsoid
(a_ν^0, b_ν^0)	expansion coefficients of the incident field
D_{mn}	normalization constant
e	north-south roundedness of superellipsoid
$\mathbf{E}_0, \mathbf{E}_s$	incident and scattered fields
(\mathbf{e}, \mathbf{h})	surface current densities
(f_ν^0, g_ν^0)	expansion coefficients of the scattered field
k	wavenumber
$\{M_{mn}^{1,3}, N_{mn}^{1,3}\}$	localized vector spherical functions
$\{\mathcal{M}_{mn}^{1,3}, \mathcal{N}_{mn}^{1,3}\}$	distributed vector spherical functions

$\{\mathcal{M}_{ni}^{1,3}, \mathcal{N}_{ni}^{1,3}\}$	magnetic and electric dipoles
$\{\mathcal{M}_n^{1,3}, \mathcal{N}_n^{1,3}\}$	vector Mie potentials
M	refractive index
n	east-west roundedness of superellipsoid
S	particle surface
$[T]$	transition matrix
(x, y, z)	cartesian coordinate
\mathbf{x}	position vector
$\alpha_n^\pm(\mathbf{x})$	Green function
α, β, γ	Euler angles
(ϑ, φ)	angular coordinates
ε	permittivity
λ_0	wavelength in vacuum
μ	permeability
v_i	vertex points on particle surface
CAD	computer aided design
DDA	discrete dipole approximation
DSCS	differential scattering cross section
DOS	disk operating system
DSM	discrete sources method
FDTD	finite difference time domain
FORTTRAN	formular translator
MMP	multiple multipole program
POV-Ray	persistance of vision raytracer
T-matrix	transition matrix
VIEM	volume integral equation method
VRML	virtual reality modelling language

10 References

- [1] *T. Wriedt*: A review of elastic light scattering theories. Part. Part. Syst. Charact. 15 (1998) 67–74.
- [2] *A. R. Jones*: Light scattering for particle characterization. Progress in Energy and Combustion Science 25 (1999) 1–53.
- [3] *B. T. Draine, P. J. Flatau*: Discrete-dipole approximation for scattering calculations. Optical Society of America: J. Opt. Soc. Am./A. 11 (1994) 1491–1499.
- [4] *D.-P. Lin, H.-Y. Chen*: Volume integral equation solution of extinction cross section by raindrops in the range 0.6–100 GHz. IEEE Transactions on Antennas and Propagation. 49 (2001) 494–499.
- [5] *W. Sun, Q. Fu, Z. Chen*: Finite-difference time-domain solution of light-scattering by dielectric particles with a perfectly matched layer absorbing boundary condition. Appl. Opt. 38 (1999) 3141–3151.
- [6] *P. Yang, K. N. Liou, M. I. Mishchenko, B.-C. Gao*: Efficient finite-difference time-domain scheme for light scattering by dielectric particles: application to aerosols. App. Opt. 39 (2000) 3727–3737.
- [7] *P. W. Barber and S. C. Hill*: Light Scattering by Particles: Computational Methods (World Scientific, Singapore, 1990).
- [8] *M. I. Mishchenko, L. D. Travis*: Capabilities and limitations of a current FORTRAN implementation of the T-matrix method for randomly oriented, rotationally symmetric scatterers. J. Quantitative Spectroscopy & Radiative Transfer. 60 (1998) 309–324.
- [9] *P. C. Waterman*: New formulation of acoustic scattering. J. Acoust. Soc. Am. 45 (1969) 1417–1429.
- [10] *P. C. Waterman*: Symmetry, unitarity and geometry in electromagnetic scattering. Phys. Review D 3 (1971) 825–839.
- [11] *P. C. Waterman*: Matrix formulation of electromagnetic scattering. Proc. IEEE 53 (1965) 805–812.
- [12] *M. I. Mishchenko*: Light scattering by randomly oriented axially symmetric particles. J. Opt. Soc. Am. A 8 (1991) 871–882.
- [13] *B. Peterson, S. Ström*: T-matrix for electromagnetic scattering from an arbitrary number of scatterers. Phys. Rev. D 8 (1973) 3661–3678.
- [14] *D. W. Mackowski*: Calculations of total cross sections of multiple-sphere clusters. J. Opt. Soc. Am. A 11 (1994) 2851–2861.
- [15] *D. Ngo, G. Videen, P. Chylek*: A Fortran code for the scattering of EM waves by a sphere with a nonconcentric spherical inclusion. Computer Physics Communications 99 (1996) 94–112.
- [16] *G. Videen, D. Ngo, P. Chylek, R. G. Pinnick*: Light scattering from a sphere with an irregular inclusion. J. Opt. Soc. Am. A 12 (1995) 922–928.
- [17] *Wenxin Zheng*: The null-field approach to electromagnetic scattering from composite objects: the case with three or more constituents. IEEE Trans. Antennas and Propagation 36 (1988) 1396–1400.
- [18] *T. Wriedt, A. Doicu*: Light scattering from a particle on or near a surface. Optics Communications 152 (1998) 376–384.
- [19] *A. Boström*: Scattering of acoustic waves by a layered elastic obstacle immersed in a fluid: an improved null-field approach. J. Acoust. Soc. Am. 76 (1984) 588–593.
- [20] *M. F. Iskander, A. Lakhtakia, C. H. Durney*: A new procedure for improving the solution stability and extending the frequency range of the EBCM. IEEE Trans. Antennas Propag. AP-31 (1983) 317–324.
- [21] *M. F. Iskander, A. Lakhtakia*: Extension of the iterative EBCM to calculate scattering by low-loss or loss-less elongated dielectric objects. Appl. Opt. 23 (1984) 948–953.
- [22] *R. H. T. Bates, D. J. N. Wall*: Null field approach to scalar diffraction: I General method; II Approximate methods; III Inverse methods. Phil. Trans. Roy. Soc. London A 287 (1977) 45–117.
- [23] *A. Lakhtakia, M. F. Iskander, C. H. Durney*: An iterative EBCM for solving the absorption characteristics of lossy dielectric objects of large aspect ratios. IEEE Trans. Microwave Theory Tech. MTT-31 (1983) 640–647.
- [24] *R. H. Hackman*: The transition matrix for acoustic and elastic wave scattering in prolate spheroidal coordinates. J. Acoust. Soc. Am. 75 (1984) 35–45.
- [25] *F. M. Schulz, K. Stamnes, J. J. Stamnes*: Scattering of electromagnetic waves by spheroidal particles: A novel approach exploiting the T-Matrix computed in spheroidal coordinates. Appl. Opt. 37 (1998) 7875–7896.
- [26] *A. Doicu, T. Wriedt*: EBCM with multipole sources located in the complex plane. Optics Communications 139 (1997) 85–98.
- [27] *T. Wriedt, A. Doicu*: Formulations of the EBCM for three-dimensional scattering using the method of discrete sources. J. Modern Opt. 45 (1998) 199–213.
- [28] *A. Doicu, Y. Eremin, T. Wriedt*: Acoustic and Electromagnetic Scattering Analysis using Discrete Sources. Academic Press, San Diego 2000.
- [29] *A. Doicu, T. Wriedt*: Extended boundary condition method with multipole sources located in the complex plane. Optics Commun. 139 (1997) 85–98.

- [30] A. Doicu, T. Wriedt: Null-field method with discrete sources to electromagnetic scattering from layered scatterers. *Comput. Phys. Commun.* 138 (2001) 136–142.
- [31] A. Doicu, T. Wriedt: Calculation of the T-matrix in the null-field method with discrete sources. *J. Opt. Soc. Am. A* 16 (1999) 2539–2544.
- [32] P. W. Barber: Differential scattering of electromagnetic waves by homogeneous isotropic dielectric bodies. Ph. D. Thesis, University of California, Los Angeles 1973
- [33] J. B. Schneider, I. C. Peden: Differential cross section of a dielectric ellipsoid by the T-Matrix extended boundary condition method. *IEEE Trans. Antennas Propagat. AP* 36 (1978) 1317–1321.
- [34] T. Wriedt, A. Doicu: Formulations of the extended boundary condition method for three-dimensional scattering using the method of discrete sources. *J. Modern Optics* 45 (1998) 199–214.
- [35] T. Wriedt, U. Comberg: Comparison of computational scattering methods. *J. Quant. Spectrosc. Radiat. Transfer* 60 (1998) 411–423.
- [36] H. Laitinen, K. Lumme: T-Matrix method for general star-shaped particles: first results. *J. Quant. Spectrosc. Radiat. Transfer* 60 (1998) 325–334.
- [37] F. M. Kahnert, J. J. Stamnes, K. Stamnes: Application of the extended boundary condition method to particles with sharp edges: a comparison of two surface integration approaches. *Applied Optics* 40 (2001) 3101–3109.
- [38] S. Havemann, A. J. Baran: Extension of T-matrix to scattering of electromagnetic plane waves by non-axisymmetric dielectric particles: application to hexagonal ice cylinders. *J. Quant. Spectrosc. Radiat. Transfer* 70 (2001) 139–158.
- [39] I. D. Faux, M. J. Pratt: *Computational Geometry for Design and Manufacture*. Wiley, Chichester 1979
- [40] A. Jaklic, A. Leonardis, F. Solina: *Segmentation and Recovery of Superquadrics*. Kluwer Academic, Dordrecht 2000.
- [41] C. Müller: *Foundations of the Mathematical Theory of Electromagnetic Waves*. Springer-Verlag, New York, 1969.
- [42] J. Bloomenthal (ed.): *Introduction to Implicit Surfaces*. Morgan Kaufmann, San Francisco, 1997.
- [43] A. Pasko: Function representation and HyperFun project. In T. L. Kunii (Ed.): *Proceedings of the 17th Spring Conference on Computer Graphics*, 25th–28th April, 2001, Budmerice, Slovakia.
- [44] HyperFun Project: Language and Software for F-rep Modeling, URL: <http://www.hyperfun.org>.
- [45] A. Pasko, V. Adzhiev, A. Sourin, V. Savchenko: Function representation in geometric modeling: concepts, implementation and applications. *The Visual Computer II* (1995) 429–446.
- [46] K. Georg, J. Tausch: Some error estimates for the numerical approximation of surface integrals. *Math. Comput.* 62 (1994) 755–763.
- [47] Ch. Hafner, L. Bomholt: *The 3D Electromagnetic Wave Simulator, 3D MMP Software and User's Guide*. Wiley, Chichester 1993.
- [48] S. Hudson: The Earth-Crossing Asteroid 1998 KY26. <http://www.eecs.wsu.edu/~hudson/Research/Asteroids/ky26/>
- [49] R. Cipolla, P. Giblin: *Visual Motion of Curves and Surfaces*. Cambridge University Press, Cambridge 2000.
- [50] POV ROCK gen 1.0. <http://www.iro.umontreal.ca/~pigeon/povpage/rockgen/rockgen.html>.
- [51] SScaTT (Superellipsoid Scattering Tool) in T. Wriedt: *Electromagnetic scattering programs*. <http://www.t-matrix.de>.